Research Article
doi: 10.1590/01047760202330013286
vol(30), 2024

CERNE

Dual-polarization vegetation indices for the Sentinel-1 sar sensor and its correlation to forest biomass from Atlantic Forest fragments

Erli Pinto dos Santos[1]✤, Isabel Caligiorne Santos[1], Jales de Freitas Bussinguer[2], Renata Ranielly Pedroza Cruz[1], Cibele Hummel do Amaral[3], Demetrius David da Silva[1], Michel Castro Moreira[1]

[1]Federal University of Viçosa, Brazil
[2]University of Brasilia, Brazil
[3]University of Colorado Boulder, United States of America

FOREST MANAGEMENT

ABSTRACT

Background: Vegetation indices have recently been proposed for remote sensing SAR (synthetic aperture radar) sensor measurements to monitor vegetation. However, they still lack validation studies on different vegetation types for their correct application. Thus, the objective of this study was to test the applicability of the Dual-polarization SAR Vegetation Index (DPSVI) and the modified DPSVI (DPSVIm) as indicators of aboveground biomass (AGB) from dense forest fragments.

Results: Three forest fragments, comprising 54 forest plots with AGB ranging from 12 up to 220 Mg ha^{-1}, were studied. These forest fragments belong to the Brazilian Atlantic Forest biome, and were located within the Doce river hydrographic basin in the state of Minas Gerais, Brazil. AGB was compared with the DPSVI and DPSVIm indices, computed from dual-polarization Sentinel-1 images, using Spearman's rank correlation test through two approaches. In the first approach (A1), correlation tests were performed using all forest plots; in the second approach (A2), samples were taken from plots on flat to undulating terrain slopes. The correlation of AGB with DPSVI presented no significant correlation (p-value >> 0.05). In contrast, for DPSVIm, the correlation with AGB was significant and positive, with coefficients ranging from 0.4 in approach A1 to 0.7 in approach A2.

Conclusion: While the DPSVI index did not show a correlation with the AGB of the studied forests, even though it is a C-band index, the DPSVIm was found to be a good indicator of the amount of AGB in forests and therefore has potential for applications in future studies, particularly in areas with reasonable slope or flat terrain.

Keywords: aboveground biomass, forest inventory, microwave remote sensing, semi decidual forest, slopes.

HIGHLIGHTS

Radar remote sensing provides important data for forest monitoring.
We tested the dual-polarization SAR vegetation indices (DPSVI and modified DPSVI).
Modified DPSVI (DPSVIm) showed to be correlated with forest aboveground biomass.
C-band SAR data can be utilised in forest monitoring.

SANTOS, E. P. D.; SANTOS, I. C.; BUSSINGUER, J. D. F.; CRUZ, R. R. P.; AMARAL, C. H. D.; SILVA, D. D. D.; MOREIRA, M. C. Dual-polarization vegetation indices for the sentinel-1 sar sensor and its correlation to forest biomass from Atlantic Forest fragments. CERNE, v.30, e-103286, doi: 10.1590/01047760202430013286.

✤Corresponding author: erlipinto@gmail.com
Received: June 21/2023 Accepted: July 8/2024

Open Access
CERNE
ISSN 0104-7760
UFLA UNIVERSIDADE FEDERAL DE LAVRAS

INTRODUCTION

From crop monitoring to ecosystem dynamics, vegetation indices (VIs) calculated using multispectral remotely sensed images have been widely utilized as tools to monitor terrestrial activities (de Oliveira Maia et al., 2022; Zeng et al., 2022). VIs are mathematical models that simplify the interpretation of the complex interactions between plant organs and electromagnetic radiation. The initial conceptions of optical VIs date back to the 1970s (Rouse et al., 1973). Since then, dozens of VIs have been developed to indicate various biochemical, biophysical, and physiological parameters of vegetation (Zeng et al., 2022).

Although VIs are widely employed in various vegetation monitoring strategies, the strong influence of clouds on the scenes results in data gaps, limiting continuous vegetation monitoring. In this context, the use of synthetic aperture radar (SAR) data emerges as a suitable alternative for monitoring vegetation dynamics regardless of weather conditions. SAR sensors are active sensors that operate in the microwave region of the electromagnetic spectrum, with wavelengths in the centimeter scale. Consequently, atmospheric effects on SAR images are reduced. Microwave radiation interacts with the structural properties of vegetation, such as size, shape, roughness, and orientation, and its dielectric properties, such as water content (Flores-Anderson et al., 2019; Woodhouse, 2006). Due to these characteristics, vegetation indices derived from SAR data offer an alternative for measuring biophysical parameters of vegetation, such as aboveground biomass (Chang et al., 2018; dos Santos et al., 2021; Periasamy, 2018). The combination of SAR data and vegetation monitoring methods provides an opportunity to enhance the monitoring of crops, forests, and other ecosystems (Bhogapurapu et al., 2021; Flores-Anderson et al., 2019).

Recently, the increasing availability of free SAR data, particularly from the European Space Agency's (ESA) C-band Sentinel-1 mission, has facilitated the development of multiple dual-polarization SAR VIs (Chang et al., 2018; dos Santos et al., 2021; Mandal et al., 2020; Nasirzadehdizaji et al., 2019; Periasamy, 2018). These VIs utilize the polarimetric features of the C-band radar signal's interaction with vegetation canopies to enhance contrast between vegetation and other distributed targets, thereby simplifying SAR data interpretation (Bussinguer et al., 2024).

Among these indices, we highlight the Dual-Polarization SAR Vegetation Index (DPSVI) (Periasamy, 2018). DPSVI is an empirical proxy for measuring the extent to which the three-dimensional and complex structure of vegetation's leaves and branches changes the polarization of C-band microwaves (which have a wavelength of approximately 5.4 cm). DPSVI, however, does not use a parameter such as the degree of polarization (Chang et al., 2018; Chang and Oh, 2007; Woodhouse, 2006). Instead, it utilizes the Euclidean distance between the backscattering coefficients of the VV and VH polarizations to distinguish bare soil pixels from those of vegetation and water bodies. Subsequently, the index separates vegetation pixels from water body pixels using a cross-ratio approach between the VH and VV polarization. Finally, the index employs the VH polarization as an indicator of signal depolarization caused by vegetation.

De Jesus et al. (2023) used DPSVI, among other SAR data, to estimate aboveground biomass (AGB) of plots in the Caatinga biome in Brazil during the green, intermediate, and dry periods. The authors found that DPSVI was an important vegetation descriptor for Caatinga vegetation, as it was included in the AGB equations for all three periods. In the dry period, DPSVI and the backscattering coefficient VH constituted the best combination for modelling the plots' AGB.

Models such as DPSVI, which utilize C-band radar data, have limitations when mapping areas with dense biomass vegetation, such as forested regions (Joshi et al., 2017). The interactions between the C-band signal and densely vegetated areas are mostly confined to the upper part of the canopy (Omar et al., 2017), where the signal tends to saturate beyond this stratum. With this in mind, dos Santos et al. (2021) proposed modifications to the mathematical formulation of the DPSVI, incorporating terms that enhance the capacity of the modified index to map forested areas, thereby reducing the effects of signal saturation.

Bussinguer et al. (2024) studied the temporal performance SAR VIs in distinguishing three different phytogeographical classes of the Cerrado within a protected area. Regarding DPSVI and DPSVIm, the authors found that both indices could describe the seasonal influences on the vegetation, but DPSVIm provided improved separability compared to DPSVI in both the wet and dry seasons. Dos Santos et al. (2021) tested the agreement of DPSVI and modified DPSVI (DPSVIm) with the optical index for forest areas, the Enhanced Vegetation Index (Huete et al., 2002), in plots of the Atlantic Forest, and observed a better correlation of EVI with DPSVIm than with DPSVI.

Areas of the Atlantic Forest are important for this kind of study due to the amount of biomass in the aboveground vegetation that forests can store, which can reach up to 663 Mg ha^{-1} (Lindner, 2010). These are areas where the density of AGB is high. There is a lack of studies testing, with field measurements, the applicability of the recently developed dual-polarization SAR vegetation indices, including in regions (or vegetation types) different from those where they were created. This leaves a gap in knowledge regarding not only their advantages and limitations but also which plant biological parameters the indices are intended to represent.

Thus, in this work, we hypothesize that DPSVIm will show a better correlation with the AGB of Atlantic Forest plots than DPSVI. Therefore, the aim of the present study is to test the applicability of both DPSVI and DPSVIm as indicators of AGB in Brazilian Atlantic Forest fragments, aiming to elucidate the theoretical background of the indices for Sentinel-1 observations.

MATERIAL AND METHODS

Description of the studied forest fragments

Three Atlantic Forest fragments were selected in this study, based on the availability of field measurements

made through a forest inventory (Tavares Júnior et al., 2020). The fragments used in this study were São José, Ipaba, and Cachoeira das Pombas, which belong to the phytogeographical region of Seasonal Semideciduous Forest (Subcaducifolia Tropical Forest) according to the IBGE (2004) and to the ecoregion of Tropical and Subtropical Moist Broadleaf Forests (Olson and Dinerstein, 1998). All of these fragments are located in the Doce river hydrographic basin, Southeast Brazil (Figure 1). The forest fragments São José, Ipaba, and Cachoeira das Pombas, are situated in the municipalities of Coronel Fabriciano, Ipaba, and Guanhães, respectively, all inside the Brazilian state of Minas Gerais.

One of the main characteristics of the basin, important for SAR imaging, is the presence of areas with high slopes, with relief ranging from nearly level and gently undulating (in the valleys and coast zone) to strongly undulating and mountainous areas (relief classes (Santos et al., 2018)). This is due to the impact of topography on modulating the backscattered microwaves, even generating radiometric distortions (Saatchi, 2019; Small, 2011). In such cases, after proper radiometric terrain corrections (Small, 2011), methodologies for plant monitoring that work in such relief conditions could be tested elsewhere.

The São José fragment has 38.4 ha (hectares) and altitudes ranging from 450 to 950 m. The Ipaba fragment is subdivided into an area of 264 ha, with altitudes ranging from 200 to 450 m, and an area of 37.3 ha, with altitudes between 150 to 300 m. The Cachoeira das Pombas fragment has 106 ha and altitudes ranging from 800 to 1,162 m.

Obtaining aboveground biomass from forest plots

In the forest fragments, permanent rectangular plots (10 x 50 m) with an area of 0.05 ha were delimited. In the São José, Ipaba, and Cachoeira das Pombas fragments, 12, 22, and 20 plots were allocated and mapped, respectively (Figure 1). The forest inventories were conducted in the year 2017 on the following dates: São José, between July 20 and August 02; Ipaba, between August 08 and 29; and Cachoeira das Pombas, between September 13 and October 02.

In each of the plots, the scientific nomenclature, the CBH (circumference at 1.30 m height, in cm), DBH (diameter at 1.30 m height, in cm), and the total plant height (H, in m) of all trees with CBH greater than or equal to 15 cm were collected. The H and DBH values obtained were set as inputs to the allometric equation (Equation 1), in order to obtain the aboveground biomass (AGB, in Kg) (dos Santos et al., 2021) of each sampled tree.

$$AGB(tree) = 0.02453 \cdot (DBH(tree)^{0.2443356}) \cdot (H(tree)^{0.423602}) \quad (1)$$

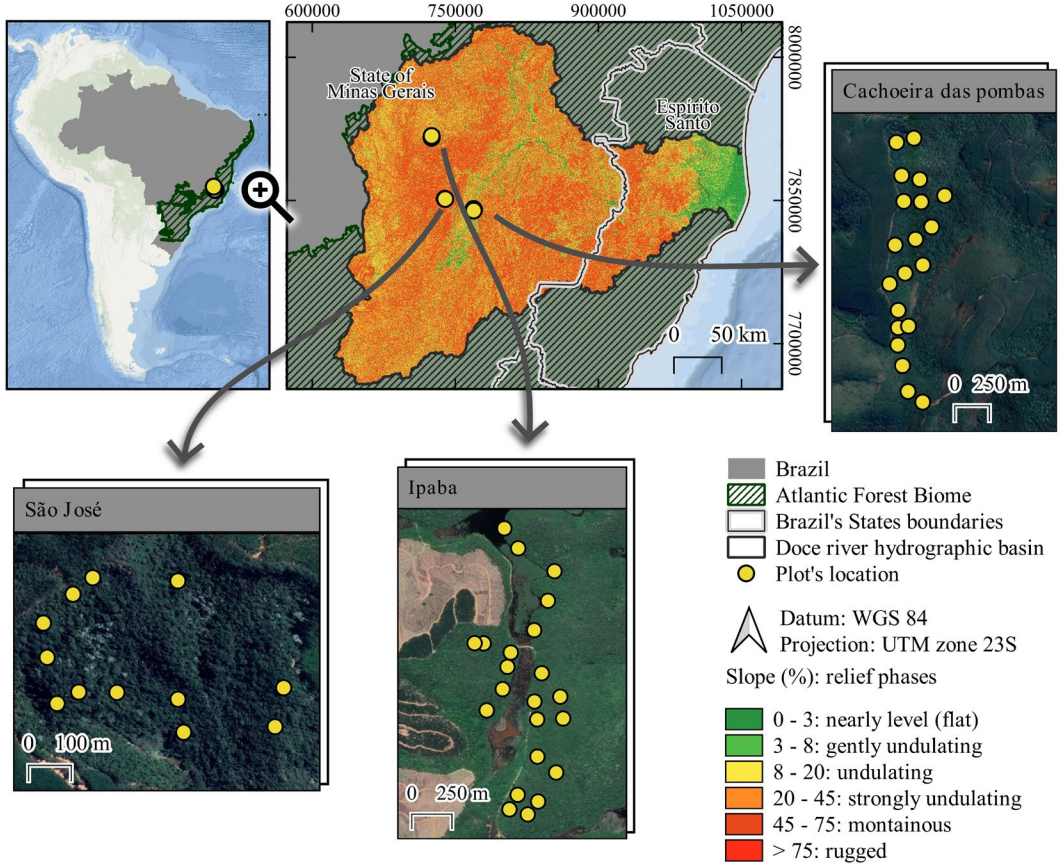

Figure 1: Location of the Atlantic Forest fragments in the Doce river hydrographic basin, Brazil. Digital Slope Model: derived from NASADEM.

The calculations of the AGB of each tree were added together to obtain the total AGB of each plot, and then converted to AGB in Mg ha^{-1}, by dividing the value found by the area of the plots.

Sentinel-1 mission imagery acquisition and processing

Images from the Sentinel-1 radar mission were used in the study (Table 1) and were obtained according to the dates of the forest inventories described in the previous topic. Dual-polarization images, set on VV and VH polarizations, obtained via the Interferometric Wide Swath imaging mode (IW) from Ground Range Detected (GRD) products, generated by the Sentinel-1B satellite, were used. Sentinel-1 IW GRD images are formed after the sensor scans the Earth's surface in three sub-swaths: IW1, IW2, and IW3; with incidence angles of 32.9°, 28.3°, and 43.1° and azimuthal resolution (spatial resolution in relation to the flight direction of the satellite) of 22.4, 22.5, and 22.6, respectively (ESA, 2022). The images were obtained from the Alaska Satellite Facility – ASF (ASF, 2023).

Imaging processing was performed to generate the bands with backscattering coefficient calibrated to *gamma_naught* (γ^0_{VV} and γ^0_{VH}), and for this, the following algorithms were applied: **1)** Subset: to crop the scenes to the area of interest, i.e., the coverage area of the three forest fragments; **2)** Apply Orbit File: to correct the orbit vector (satellite position and speed) with accurate post-processed data (by the control segment); **3)** Thermal Noise Removal: for removing thermal noise from the antenna itself; **4)** Border Noise Removal: to remove noisy edges from the images; **5)** Radiometric Calibration: to normalize the observed wave amplitude in each band to a section (Radar Cross Section) and obtain the backscattering coefficient (reflectivity per unit area) in β^0 (the normalized backscattering coefficient without a Earth surface model, projected section necessary to perform terrain corrections); **6)** application of a Speckle Noise removal filter: the Lee Sigma adaptive filter was applied, with a 11 x 11 pixel window: Lee Sigma was chosen because it is a standard deviation-based filter, which performs filtering based on statistics calculated from the data, preserving image sharpness and detail while suppressing noise (Meyer, 2019); **7)** Radiometric Terrain Flattening with *oversamplingMultiple* = 4.0: whose goal was to attenuate backscattering distortions caused by relief artifacts (hills, steep slopes, mountains, etc.) and where the backscattering coefficient was converted from β^0 to γ^0 (the backscattering coefficient after radiometric terrain correction with terrain Earth model) according to Small (2011) methodology; **8)** which consisted of orthorectifying the images with the Range-Doppler Terrain Correction algorithm, in which the output pixel dimensions was set to 10 m.

Computation of Sentinel-1 SAR vegetation indices

The Dual-polarization SAR Vegetation Index (DPSVI) and the modified DPSVI (DPSVIm) vegetation indices were calculated using the VH and VV polarization bands. The values of the VH and VV bands were calibrated to γ^0 in linear power units.

The DPSVI index is the product of two other indices and the VH band. The IDPDD (Inverse Dual-pol Diagonal Distance) and the VDDPI (Vertical Dual-pol Index) indices are calculated by (Equations 2, 3), respectively (Periasamy, 2018):

$$IDPDD_{(i,j)} = \frac{\left(VV_{\max} - VV_{(i,j)}\right) + VH_{(i,j)}}{\sqrt{2}} \quad (2)$$

$$VDDPI_{(i,j)} = \frac{VV_{(i,j)} + VH_{(i,j)}}{VV_{(i,j)}} \quad (3)$$

Where $VV_{(i,j)}$ and $VH_{(i,j)}$ are the VV and VH band values, respectively, in the pixel at the coordinate (i,j).

By multiplying IDPDD by VDDPI and the VH band gives the value of DPSVI, which was obtained by (Equation 4):

$$DPSVI_{(i,j)} = IDPDD_{(i,j)} VDDPI_{(i,j)} VH_{(i,j)} \quad (4)$$

The VV_{max} parameter was defined by exploring the VV versus VH scatterplot of the three used scenes. In this study, the VV_{max} parameter was set equal to 1.5. This value of VV was set following recommendations of Periasamy (2018), which states that VV_{max} must to encompass the natural surface scatterer pixels (water, uncovered soil, and plants) in a triangle where the VV and VH measurements are concentrated (Figure 2).

The DPSVIm index is the product of the DPDD (Dual-pol Diagonal Distance, (Equation 5) and Cross-ratio (CR) (Equation 6)) indices and the VH band:

$$DPDD_{(i,j)} = \frac{VV_{(i,j)} + VH_{(i,j)}}{\sqrt{2}} \quad (5)$$

$$CR_{(i,j)} = \frac{VV_{(i,j)}}{VH_{(i,j)}} \quad (6)$$

Table 1: Inventory of Sentinel-1 IW GRD images used in the study.

Acquisition date	Product Unique Identifier	Relative Orbit Number	Forest fragment	Rainfall (mm)*
July 26, 2017	495B		São José	0.2
August 31, 2017	6D51	155	Ipaba	0.0
September 24, 2017	F6D1		Cachoeira das Pombas	0.0

*Total rainfall on the same day plus in one week before the date of the acquired image, measured in the nearest rain gauge.

Where $CR_{(i,j)}$ is the Cross-Ratio of VV to VH band.

By multiplying DPDD, CR, and VH band, it gives the value of DPSVIm, which was calculated using (Equation 7):

$$DPSVIm_{(i,j)} = DPDD_{(i,j)}CR_{(i,j)}VH_{(i,j)} \quad (7)$$

The software codes used in this work, to handle Sentinel-1 IW GRD products, were developed by dos Santos et al. (2023) and are hosted in public repository. The scripts were developed in Python programming language, for Sentinel-1 IW GRD images processing, and in R language (R Core Team, 2023), for both raster sampling according to the forest plots and statistical analysis.

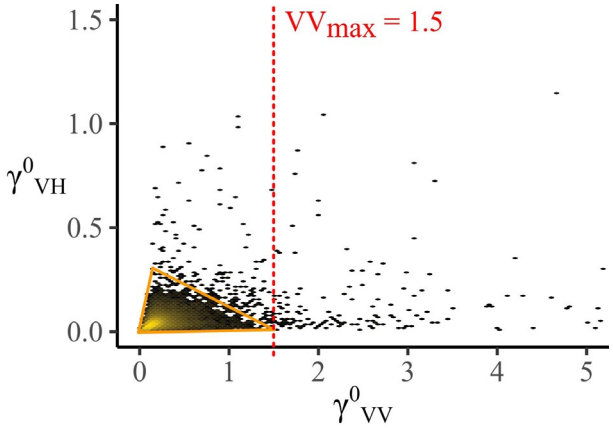

Figure 2: Scatterplot between VV and VH bands showing the maximum VV value adopted for the DPSVI calculation and the approximation of a triangle representing soil, water, and vegetation pixels. Product Unique Identifier: 495B.

Comparative performance analysis of vegetation indices

The VH polarization, the DPSVI, and DPSVIm indices were compared with AGB of all forest plots using correlation test. The correlation test used was Spearman's ranks test. This test was chosen after having tested the normality of the variables by the Shapiro-Wilk normality test. With this one, it was detected the AGB dataset do not follow a normal distribution (Figure 3).

For the correlation test, the null hypothesis (H_0) is that there is no linear relationship between the two tested variables. The alternative hypothesis (H_a) states that there is a linear relationship between the two variables. The confidence interval for interpreting the correlation (and normality) was 95% (a significance level of).

Due to the influence that topography has on side-looking imaging, which is fundamental for SAR antenna sensing, two approaches to test the correlation between the indices were performed. In the first approach (A1) all samples were used together. In the second approach (A2), only samples from plots with nearly level, gently undulating, and undulating relief phases were used to test the correlation of the indices with AGB.

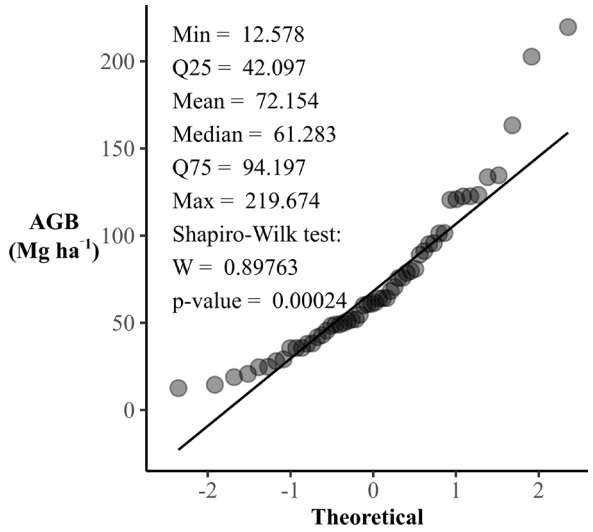

Figure 3: Quantile distribution plot of aboveground biomass (AGB) showing the statistical metrics of central tendency and dispersion of all the forest plots, as well as the results of the Shapiro-Wilk normality test.

RESULTS

The range of AGB values for the studied forest plots varied from 12.6 to 219.7 Mg ha^{-1} (Table 2). In contrast, the values for Sentinel-1 VH polarisation varied on a different scale from AGB, ranging from approximately 0.01 to 0.09 (in linear power units scale). Comparatively, the Sentinel-1 derived indices, namely DPSVI and DPSVIm, exhibited similar ranges. These findings underscore the importance of conducting correlation tests to evaluate the relationship between dual-polarisation SAR vegetation indices and forest AGB.

Spearman's correlation tests were conducted between AGB and VH polarisation, the DPSVI, and the DPSVIm indices in both approaches (A1 and A2). In approach A1, there was no significant correlation between AGB and VH polarisation, as indicated by a p-value of 0.7392, as shown in Figure 4a. Similarly, there was no significant correlation between AGB and the DPSVI (p-value = 0.27252, Figure 4b). However, the correlation test between AGB and the DPSVIm yielded a p-value of 0.00339, leading to the rejection of the null hypothesis and suggesting a significant correlation between AGB and the DPSVIm.

In approach A1, the correlation between AGB and the DPSVIm was ρ = 0.394 (Figure 4c). However, this correlation coefficient was higher in approach A2.

In the approach A2, correlation tests between AGB and VH polarization and AGB and DPSVI remained with no significant effect (refer to Figure 5a and Figure 5b). However, the correlation coefficient of the test between AGB and DPSVIm increased from $\rho \cong 0.4$ (in the correlation test for approach A1) to ρ = 0.713, in the approach A2 (see Figure 5c). The difference between correlation tests in approaches A1 and A2 lies in the former's use of all samples from all forest plots together. Conversely, in approach A2, forest plot samples were filtered, and only samples from plots with nearly flat relief

(including gently undulating and undulating phases) were used to compare the SAR variables and the AGB.

When comparing the correlation of AGB versus DPSVI, as well as VH polarization, in approaches A1 (Figure 4a and b) and A2 (Figure 5a and b), we noticed that although AGB values vary from 20 to 220 Mg ha^{-1}, DPSVI and VH polarization values consistently hover around 0.05, exhibiting no significant correlation with AGB (adjusted p-values >> 0.05). Conversely, upon filtering the samples by the relief of the forest plot, the correlation of DPSVIm with AGB increased from ρ = 0.4 to ρ ~ 0.7, indicating a strong correlation that remained statistically significant (p – value < 0.05).

DPSVI and DPSVIm share the same conceptual design; both were developed based on the depolarisation effect of microwave signals by vegetation. Therefore, the difference in observed correlation with AGB between the two indices can be attributed to the modifications introduced in DPSVIm. From DPSVI to DPSVIm, two internal indices were altered: the IDPDD was replaced by the DPDD, and the VDDPI was substituted with the CR.

Figure 6 depicts scatterplots between DPDD *vs*. IDPDD (Figure 6a) and CR *vs*. VDDPI (Figure 6b) obtained from Sentinel-1 scene 495B. The other two Sentinel-1 products were not included due to their similarity to scene 495B.

The DPDD and IDPDD exhibit an inversely proportional relationship with each other, as depicted in Figure 6a. Also, the inversely proportional relationship of DPDD and IDPDD holds similar range of values. However, in the case of the DPSVI, the depolarization index VDDPI has been substituted with the CR.

The CR and VDDPI indices display an inversely proportional relationship, with the CR demonstrating exponential behaviour. As VDDPI values decrease towards zero (from 3.0), CR values increase towards 25 (from zero). This implies that the VV polarization has a greater influence on the DPSVIm index, which tends to better reflect the signal backscattered by broadleaf vegetation.

Figure 7 displays the computed DPSVIm maps for each forest fragment along with the locations of the forest plots. Additionally, on the left side of the DPSVIm maps, the relative composition of Sentinel-2 images in natural colour is presented. In Figure 7, it is evident that the lowest DPSVIm values (near zero) correspond to water bodies, while low DPSVIm values are observed in unforested areas, whether with or without bare soil.

In Figure 7, forest plots were positioned at their centroids and depicted by circles, with size increasing as AGB (Mg ha^{-1}) increases. Additionally, in Figure 7, we observed that the smallest circles correspond to the darkest

Table 2: Descriptive statistics for the obtained variables: Aboveground Biomass (AGB, Mg ha^{-1}), Sentinel-1 VH polarization (γ^0_{VH}), Dual-Pol SAR Vegetation Index (DPSVI), and the modified DPSVI (DPSVIm).

Variable	Min	Q_{25}	$\bar{x}$	sd	Md	Q_{75}	Max	Shapiro-Wilk test		s
								W	p-value	
AGB (Mg ha^{-1})	12.6	42.1	72.2	44.5	61.3	94.2	219.7	0.898	0.000235	1.32
	0.01249	0.03758	0.04420	0.01147	0.04316	0.04775	0.08915	0.872	0.000035	1.32
DPSVI	0.01967	0.04478	0.05463	0.01636	0.05133	0.06199	0.12796	0.857	0.000013	1.92
DPSVIm	0.00067	0.02026	0.02735	0.01276	0.02368	0.03140	0.07733	0.839	0.000004	1.79

Note: Min, Q_{25}, $\bar{x}$, sd, Md, Q_{75}, and Max refers to the minimal, quantile 25%, mean, standard deviation, median, quantile 75%, and maximum values obtained from each described variable's distribution; W and p-value refers to the statistics from Shapiro-Wilk normality test; and s refers to the skewness distribution coefficient.

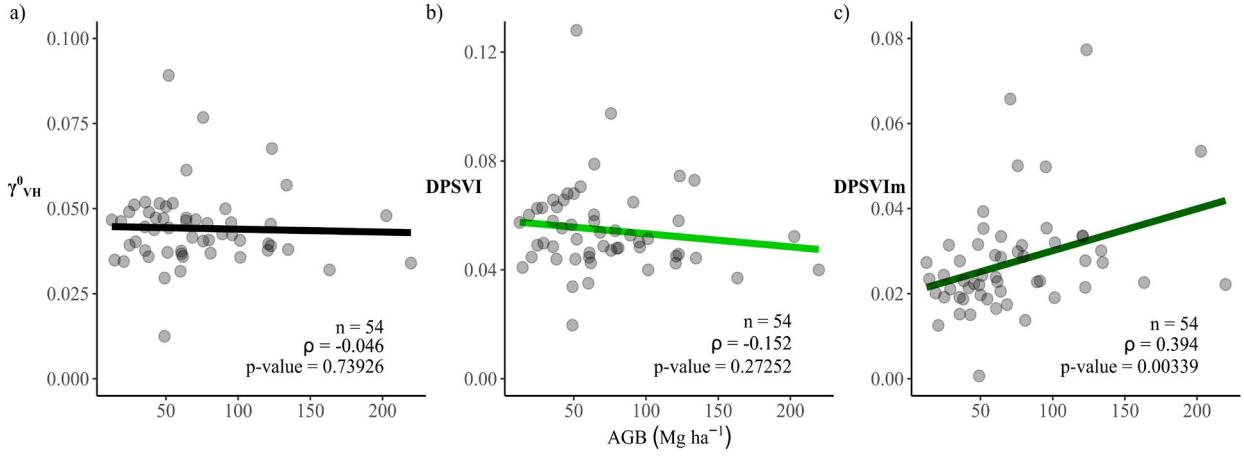

Figure 4: Scatterplot and the result of the correlation test for approach A1, between aboveground biomass (AGB) and: the Sentinel-1 VH polarization (γ^0_{VH}) in plot a); the Dual-polarization SAR Vegetation Index (DPSVI) in plot b); the modified DPSVI (DPSVIm) in plot c).

DPSVIm regions, while the largest circles are positioned near o precisely over the brightest DPSVIm regions.

DISCUSSION

Typically, C-band measured backscattering tends to saturate at approximately 50 Mg ha^{-1} of AGB (Joshi et al., 2017; Sarker et al., 2013), however, dos Santos et al. (2021) have already observed that with the DPSVIm index it was possible to distinguish plots with biomass levels less than 50 Mg ha^{-1} from others with AGB density around 200 Mg ha^{-1}, as can be seen in Figure 4 and in Figure 5. Therefore, even being a C-band index, DPSVIm tends to attenuate signal saturation over areas of dense biomass, such as the Atlantic Forest.

The correlation test using the A2 approach was performed bearing in mind the influence of relief on SAR side-looking observation systems. Relief artifacts, depending on the slope steepness and sensor parameters, generate geometric distortions in SAR images (Vollrath et al., 2020), which influence vegetation mapping and biomass quantification (Atwood et al., 2014). While radiometric terrain flattening (RTF) method can significantly enhance the radiometric accuracy of SAR images, it does not completely solve all geometric effects on backscattering (Small, 2011). Therefore, reasonable slope or flat terrain areas are recommended for this type of test (Saatchi, 2019).

Calibrating the images for the gamma backscattering coefficient (γ^0), which is important to apply to analyze SAR remote sensing products in steep areas, mitigates the influence of steep terrain on SAR imaging, but does not resolve all geometric effects of the relief (dos Santos et al., 2021; Vollrath et al., 2020). Therefore, we observed a gain in correlation coefficients in the DPSVIm index when confronting the index with AGB in less sloping areas (with steepness slope inferior to 20%), which indicates a good correlation of DPSVIm data with AGB.

The structure of the proposed modifications to the DPSVI model was carried out to decrease the computational demand for image processing, since several operations are performed with Sentinel-1 images. Furthermore, dos Santos et al. (2021) sought to deal with the uncertainty associated with the choice of the parameter VV_{max} for DPSVI application in vegetation mapping in large hydrographic basins (the Doce river basin).

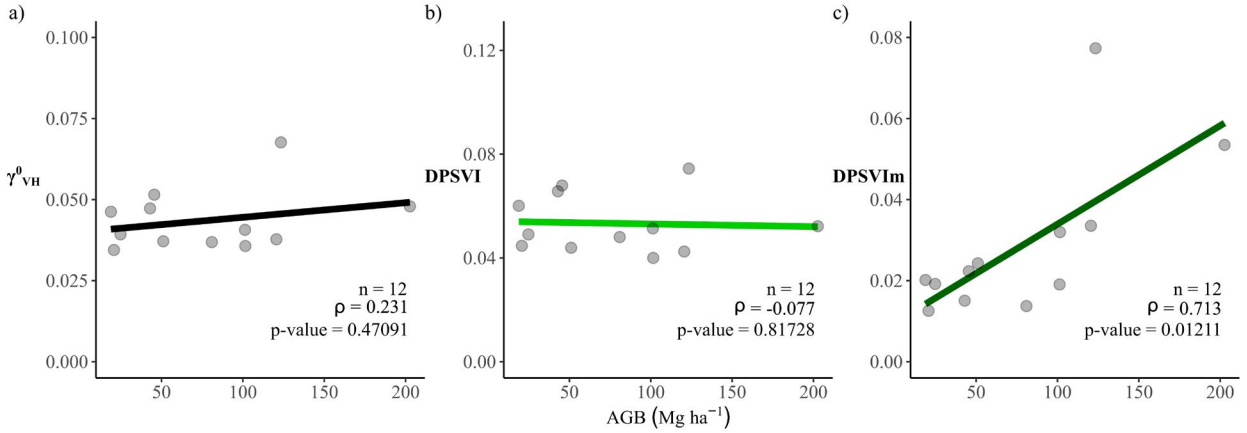

Figure 5: Scatterplot and the result of the correlation test for approach A2, between aboveground biomass (AGB) and: the Sentinel-1 VH polarization (γ^0_{VH}) in plot a); the Dual-polarization SAR Vegetation Index (DPSVI) in plot b); the modified DPSVI (DPSVIm) in plot c). Only forest plot samples from nearly level, gently undulating, and undulating terrain were used in these scatterplots.

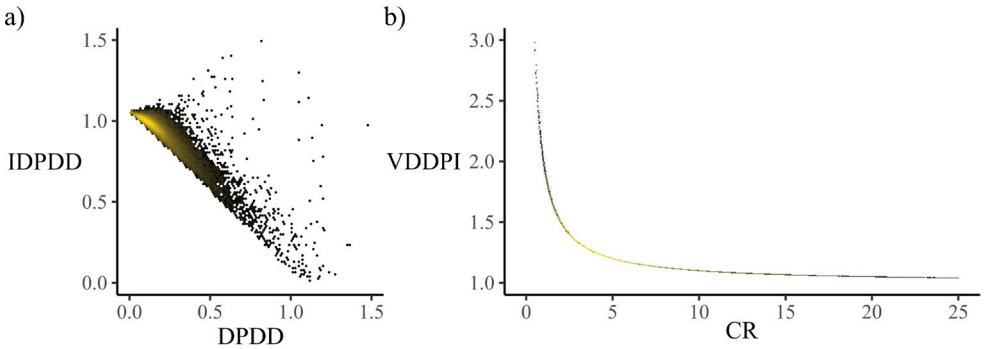

Figure 6: Scatterplots: in a) between DPDD (Dual-polarization Diagonal Distance) and IDPDD (Inverse DPDD) indices; and in b) between the CR (Cross-ratio) and VDDPI (Vertical Dual-depolarization Index) indices. Product Unique Identifier: 495B.

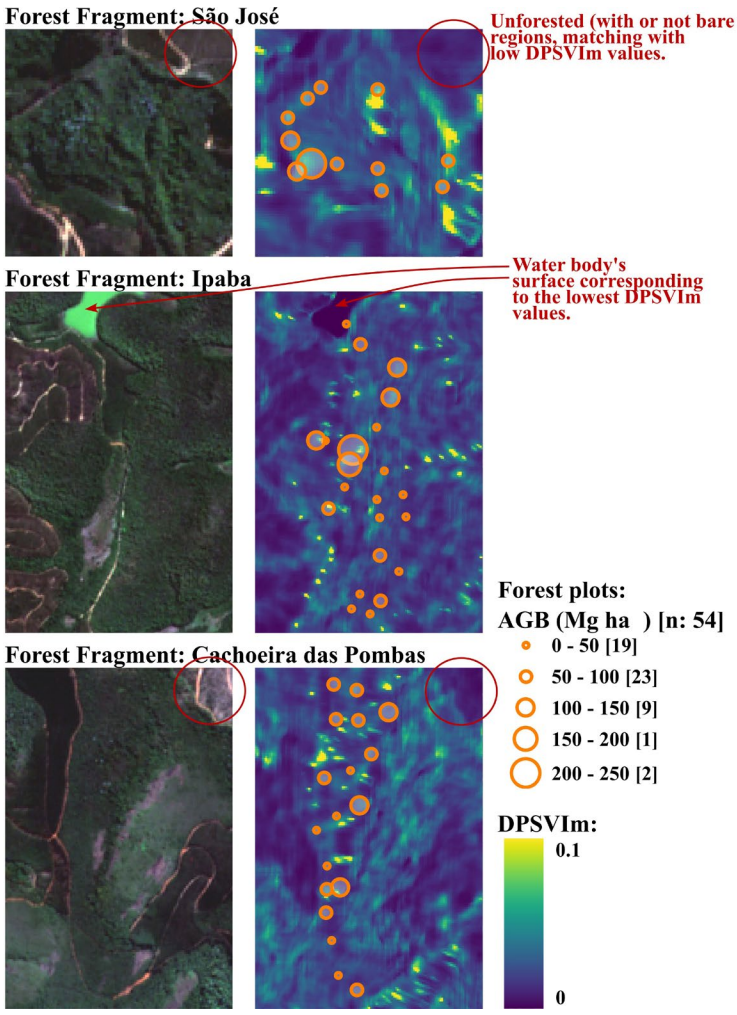

Figure 7: Modified Dual-polarisation SAR Vegetation Index (DPSVIm) maps for each studied forest fragment and relative natural colour composition from Sentinel-2 optical images. Forest plots are represented with points whose size varies according to aboveground biomass (AGB) density.

By replacing the inverse diagonal distance (between the VV and VH) (IDPDD) with the diagonal distance (DPDD) (both from Periasamy (2018)), an advantage arises in the use of DPSVIm: the need for the remote sensing expert to analyze the scatterplots (VV *vs.* VH) of all scenes in search of a representative VV_{max} becomes dispensable.

This advantage eliminates the need to analyze a large number of scatterplots when the index is applied for mapping large areas. But, as the IDPDD and DPDD have an inversely proportional relationship (Figure 6a), the term VDDPI was also replaced to maintain the scale of the DPSVIm: $0 < DPSVIm$, increasing as plant biomass increases.

The VDDPI index represents, for DPSVI, the measure of depolarization of the microwave signal (Periasamy, 2018). The highest VDDPI values represent the surface targets that do not change the polarization of the signal, such as continental water surfaces and bare soil. These are natural targets that, depending on roughness, generate the single bounce backscattering mechanism (Woodhouse, 2006). Hence, when VDDPI is integrated with IDPDD, the bare soil and water surface pixels are separated from the other pixels representing vegetation (Periasamy, 2018).

The VDDPI was replaced with the CR value, used by Frison et al. (2018) to monitor deciduous oak (*Quercus* spp.) forests, because they are inversely proportional (Figure 6b). The smaller CR values represent scatterers that do not much change the wave polarization, but in addition, when the VV band is the numerator of the cross-ratio (Equation (6)), a greater weight is given to surface scattering from leaves and branches in the upper part of the deciduous forest canopy (Frison et al., 2018). Hence CR, in addition to being inversely proportional to VDDPI, still stratifies dense vegetation pixels better than VDDPI. In Figure 5b it can be seen that the range of VDDPI is from 1.0 to 3.0 while CR ranges from 0.0 to 25.

The presented results (Figure 4, Figure 5, and Figure 7) show the applicability of Sentinel-1 dual-polarization observations for forestry applications. Although the original model, DPSVI, does not correlate well with forest AGB, there was a correlation gain with the modifications performed to propose DPSVIm.

Different optical vegetation indices with different purposes (Zeng et al., 2022) can be used in ensembles to monitor different aspects of vegetation, and the same is true for SAR vegetation indices. Recently other indices have been developed to identify the phenological stages of crops (Bhogapurapu et al., 2021, 2022; Mandal et al., 2020) and the phenology of forests (Frison et al., 2018). DPSVI itself has already shown efficiency in representing crops' AGB (Periasamy, 2018) and was used, together with DPSVIm, to monitor maize (*Zea mays* L.) lodging (Guan et al., 2022). VH polarization, DPSVI, and DPSVIm were also utilised jointly and effectively to model potato carbon uptake (Araujo-Carrillo et al., 2024) and to retrieve soil moisture at high spatial resolution over alpine ecosystems (Taghavi-Bayat et al., 2024). VH polarization and DPSVIm were also successfully applied in predicting alfalfa yield (Yu et al., 2024). However, for applications in areas of dense biomass, whether crops, forest plantations, or natural forests, descriptors such as CR and DPSVIm may be more efficient.

In this context, Bussinguer et al. (2024) have evaluated the efficacy of various SAR vegetation indices in discriminating vegetation classes within the Cerrado biome, Brazil. The authors employed the radar vegetation index adapted for dual-polar data (Nasirzadehdizaji et al., 2019), the Dual-polarization radar vegetation index (Mandal et al., 2020), the polarimetric radar vegetation index (Chang et al., 2018), DPSVI, and DPSVIm. They assessed three vegetation categories, namely Forest, Savanna, and Grassland. The authors observed that DPSVIm more accurately reflected biomass levels across the three vegetation types and surpassed the other indices in class differentiation.

It is essential that future studies test the sensitivity of DPSVIm in areas of dense biomass, but with different vegetation landforms than semideciduous forests. Zheng et al. (2023) effectively used DPSVIm, and other variables, to map the distribution of tree species in landscapes that include tropical rainforests, subtropical evergreen broadleaf forests, and mixed coniferous broadleaf forests. However, future studies can test the applicability of DPSVIm in similarly dense biomass areas, but with different plant architectures, such as sugarcane (*Saccharum officinarum* L.) and other monocot crops.

CONCLUSIONS

The DPSVI index showed no correlation with the AGB in Atlantic Forest plots. This demonstrates that it is insensitive to large amounts of AGB, and not a good indicator of AGB of Subcaducifolia Tropical Forest plots. The DPSVIm showed correlation coefficients varying from ρ = 0.4 to ρ = 0.7 with AGB in the same Subcaducifolia Tropical Forest plots. Hence, DPSVIm is a C-band SAR index more suitable for forest applications than the DPSVI. The higher correlation coefficient was observed with AGB of forest plots with near flat relief, indicating its potential for monitoring the AGB of forests, such as the Atlantic Forest, particularly in areas with reasonable slope or flat terrain (steepness less than 20%).

AUTHORSHIP CONTRIBUTION

Project Idea: E. P. S.; R. R. P. C.; C. H. A.; D. D. S., M. C. M.

Funding: C. H. A.

Database: R. R. P. C.

Processing : E. P. S.; I. C. S.; J. F. B.; M. C. M.

Analysis : E. P. S.; I. C. S.; J. F. B.; R. R. P. C.; D. D. S.; M. C. M.

Writing : E. P. S.; I. C. S.; J. F. B.; D. D. S.

Review : R. R. P. C.; C. H. A.; D. D. S.

ACKNOWLEDGEMENT

We thank the Celulose Nipo-Brasileira S.A. for providing the field data. This study was financed in part by the Coordenação de Aperfeiçoamento de Pessoal de Nível Superior - Brazil (CAPES) - Finance Code 001, the Conselho Nacional de Desenvolvimento Científico e Tecnológico (CNPq), and the Fundação de Amparo à Pesquisa do Estado de Minas Gerais (FAPEMIG).

REFERENCES

ARAUJO-CARRILLO, G. A.; DUARTE-CARVAJALINO, J. M.; SÁNCHEZ-VIVAS, D. F.; et al. Using SAR-based products to calculate potato carbon uptake in a tropical Andean region. European Journal of Remote Sensing, v.57, n.1, p. 2339272, 2024. https://doi.org/10.1080/22797254.2024.2339272

ASF. (2023). Copernicus Sentinel data 2017, processed by ESA. [dataset].

ATWOOD, D. K.; ANDERSEN, H.-E.; MATTHISS, B.; et al. Impact of Topographic Correction on Estimation of Aboveground Boreal Biomass Using Multi-temporal, L-Band Backscatter. IEEE Journal of Selected Topics in Applied Earth Observations and Remote Sensing, v.7, n.8, p. 3262–3273, 2014. https://doi.org/10.1109/JSTARS.2013.2289936

BHOGAPURAPU, N.; DEY, S.; BHATTACHARYA, A.; et al. Dual-polarimetric descriptors from Sentinel-1 GRD SAR data for crop growth assessment. ISPRS Journal of Photogrammetry and Remote Sensing, v.178, p.20–35, 2021. https://doi.org/10.1016/j.isprsjprs.2021.05.013

BHOGAPURAPU, N.; DEY, S.; MANDAL, D.; et al. Soil moisture retrieval over croplands using dual-pol L-band GRD SAR data. Remote Sensing of Environment, 271, 2022. https://doi.org/10.1016/J.RSE.2022.112900

BUSSINGUER, J. DE F.; BAPTISTA, G. M. DE M.; SANO, E. E.; et al. Understanding the Spatio-Temporal Behavior of Sentinel-1 SAR Vegetation Indices Over the Brazilian Savanna. IEEE Transactions on Geoscience and Remote Sensing, v.62, p.1–18. 2024. https://doi.org/10.1109/TGRS.2024.3381468

CHANG, J. G.; OH, Y. Polarimetric SAR Image Classification Based on the Degree of Polarization and Co-polarized Phase-Difference Statistics. Asia-Pacific Microwave Conference, p.1–4, 2007. https://doi.org/10.1109/APMC.2007.4555104

CHANG, J. G.; SHOSHANY, M.; OH, Y. Polarimetric Radar Vegetation Index for Biomass Estimation in Desert Fringe Ecosystems. IEEE Transactions on Geoscience and Remote Sensing, v.56, n.12, p. 7102–7108, 2018. https://doi.org/10.1109/TGRS.2018.2848285

DE JESUS, J. B.; KUPLICH, T. M.; DE C. BARRETO, Í. D.; et al. Estimation of aboveground biomass of arboreal species in the semi-arid region of Brazil using SAR (synthetic aperture radar) images. Journal of Arid Land, v.15, n.6, p.695–709, 2023. https://doi.org/10.1007/s40333-023-0017-4

MAIA, F. C. O.; BUFON, V. B.; LEÃO, T. P. Vegetation indices as a Tool for Mapping Sugarcane Management Zones. Precision Agriculture, v. 24, p.213-234, 2023. https://doi.org/10.1007/s11119-022-09939-7

DOS SANTOS, E. P.; DA SILVA, D. D.; DO AMARAL, C. H. Vegetation cover monitoring in tropical regions using SAR-C dual-polarization index: Seasonal and spatial influences. International Journal of Remote Sensing, v.42, n.19, p.7581–7609, 2021. https://doi.org/10.1080/01431161.2021.1959955

ESA, E. S. A. Sentinel-1 SAR Technical Guide. (2022). https://sentinel.esa.int/web/sentinel/technical-guides/sentinel-1-sar

Flores-Anderson, A. I.; Herndon, K. E.; Thapa, R. B.; et al. (Eds.) The Synthetic Aperture Radar (SAR) Handbook: Comprehensive Methodologies for Forest Monitoring and Biomass Estimation. 2019. NASA. https://doi.org/10.25966/nr2c-s697

FRISON, P.-L.; FRUNEAU, B.; KMIHA, S.;et al. Potential of Sentinel-1 Data for Monitoring Temperate Mixed Forest Phenology. Remote Sensing, v.10, n.12, p.2049, 2018. https://doi.org/10.3390/rs10122049

GUAN, H.; HUANG, J.; LI, L.; et al. A Novel Approach to Estimate Maize Lodging Area With PolSAR Data. IEEE Transactions on Geoscience and Remote Sensing, v.60, p.1–17, 2022. https://doi.org/10.1109/TGRS.2022.3216341

HUETE, A.; DIDAN, K.; MIURA, T.; et al. Overview of the radiometric and biophysical performance of the MODIS vegetation indices. Remote Sensing of Environment, v.83, n.1–2, p.195–213, 2002. https://doi.org/10.1016/S0034-4257(02)00096-2

IBGE. Mapa de Vegetação do Brasil (3rd ed.) [Map]. 2004. https://geoftp.ibge.gov.br/informacoes_ambientais/vegetacao/mapas/brasil/vegetacao.pdf

JOSHI, N.; MITCHARD, E. T. A.; BROLLY, M.; et al. Understanding "saturation" of radar signals over forests. Scientific Reports, v.7, n.1, p.1–11, 2017. https://doi.org/10.1038/s41598-017-03469-3

LINDNER, A. Biomass storage and stand structure in a conservation unit in the Atlantic Rainforest—The role of big trees. Ecological Engineering, v.36, n.12, p.1769–1773, 2010. https://doi.org/10.1016/j.ecoleng.2010.07.017

MANDAL, D.; KUMAR, V.; RATHA, D.;et al. Dual polarimetric radar vegetation index for crop growth monitoring using sentinel-1 SAR data. Remote Sensing of Environment, v.247, p. 111954, 2020. https://doi.org/10.1016/j.rse.2020.111954

MEYER, F. J. Spaceborne Synthetic Aperture Radar: Principles, Data Access, and Basic Processing Techniques. In Synthetic Aperture Radar (SAR) Handbook: Comprehensive Methodologies for Forest Monitoring and Biomass Estimation. NASA. 2019.

NASIRZADEHDIZAJI, R.; BALIK SANLI, F.; ABDIKAN, S.; et al. Sensitivity Analysis of Multi-Temporal Sentinel-1 SAR Parameters to Crop Height and Canopy Coverage. Applied Sciences, v.9, n.4, p.655, 2019. https://doi.org/10.3390/app9040655

OLSON, D. M.; DINERSTEIN, E. The Global 200: A Representation Approach to Conserving the Earth's Most Biologically Valuable Ecoregions. Conservation Biology, v.12, n.3, p.502–515, 1998. https://doi.org/10.1046/j.1523-1739.1998.012003502.x

OMAR, H.; MISMAN, M. A.; KASSIM, A. R. Synergetic of PALSAR-2 and Sentinel-1A SAR Polarimetry for Retrieving Aboveground Biomass in Dipterocarp Forest of Malaysia. Applied Sciences, v.7, n.7, p.375, 2017. https://doi.org/10.3390/app7070675

PERIASAMY, S. Significance of dual polarimetric synthetic aperture radar in biomass retrieval: An attempt on Sentinel-1. Remote Sensing of Environment, v.217, p.537–549, 2018. https://doi.org/10.1016/j.rse.2018.09.003

R Core Team, R. R: A Language and Environment for Statistical Computing [Computer software]. 2023. R Foundation for Statistical Computing. https://www.r-project.org/

ROUSE, J. W.; HASS, R. H.; SCHELL, J. A.; et al. Monitoring vegetation systems in the great plains with ERTS. Third Earth Resources Technology Satellite (ERTS) Symposium, v.1, p. 309–317, 1973. https://doi.org/citeulike-article-id:12009708

SAATCHI, S. SAR Methods for Mapping and Monitoring Forest Biomass. In A. I. Flores-Anderson, K. E. Herndon, R. B. Thapa, and E. Cherrington (Eds.), The Synthetic Aperture Radar (SAR) Handbook: Comprehensive Methodologies for Forest Monitoring and Biomass Estimation. 2019 NASA. https://doi.org/10.25966/nr2c-s697

SANTOS, E. P. DOS; MOREIRA, M. C.; FERNANDES-FILHO, E. I.; et al. Sentinel-1 Imagery Used for Estimation of Soil Organic Carbon by Dual-Polarization SAR Vegetation Indices. Remote Sensing, v.15, n.23, p.5464, 2023. https://doi.org/10.3390/rs15235464

SANTOS, H. G. DOS; JACOMINE, P. K. T.; DOS ANJOS, L. H. C.; et al. Brazilian Soil Classification System (5th ed.) 2018. Embrapa. https://www.embrapa.br/en/solos/sibcs

SARKER, M. L. R., NICHOL, J., IZ, H. B., et al. Forest Biomass Estimation Using Texture Measurements of High-Resolution Dual-Polarization C-Band SAR Data. IEEE Transactions on Geoscience and Remote Sensing, v.51, n.6, p.3371–3384, 2013. https://doi.org/10.1109/TGRS.2012.2219872

SMALL, D. Flattening Gamma: Radiometric Terrain Correction for SAR Imagery. IEEE Transactions on Geoscience and Remote Sensing, v.49, n.8, p.3081–3093, 2011. https://doi.org/10.1109/TGRS.2011.2120616

TAGHAVI-BAYAT, A.; GERKE, M.; RIEDEL, B. (2024). Soil moisture retrieval at high spatial resolution over alpine ecosystems on Nagqu-Tibetan plateau: A comparative study on semiempirical and machine learning approaches. Science of Remote Sensing, v.9, p.100135. https://doi.org/10.1016/j.srs.2024.100135

TAVARES JÚNIOR, I. DA S.; TORRES, C. M. M. E.; LEITE, H. G.; et al. Machine learning: Modeling increment in diameter of individual trees on Atlantic Forest fragments. Ecological Indicators, v.117, p.106685, 2020. https://doi.org/10.1016/j.ecolind.2020.106685

VOLLRATH, A.; MULLISSA, A., REICHE, J. Angular-Based Radiometric Slope Correction for Sentinel-1 on Google Earth Engine. Remote Sensing, v.12, n.11, p. 1867, 2020. https://doi.org/10.3390/rs12111867

WOODHOUSE, I. H. Introduction to Microwave Remote Sensing. 2006. CRC Press.

YU, T.; ZHOU, J.; RANJBAR, S.; et al. Evaluation of the Effect of Sentinel-1 SAR and Environmental Factors in Alfalfa Yield and Quality Estimation. Agronomy, v.14, n.4, p.859, 2024. https://doi.org/10.3390/agronomy14040859

ZENG, Y.; HAO, D.; HUETE, A.; et al. Optical vegetation indices for monitoring terrestrial ecosystems globally. Nature Reviews Earth and Environment. v.3, p.477-493, 2022. https://doi.org/10.1038/s43017-022-00298-5

ZHENG, P.; FANG, P.; WANG, L.; et al. Synergism of Multi-Modal Data for Mapping Tree Species Distribution—A Case Study from a Mountainous Forest in Southwest China. Remote Sensing, v.15, n.4, p.979, 2023. https://doi.org/10.3390/rs15040979